Physica Scripta

PAPER

Tomographic discord for a system of two coupled nanoelectric circuits

To cite this article: A K Fedorov *et al* 2015 *Phys. Scr.* **90** 055101

IOP Publishing | Royal Swedish Academy of Sciences Physica Scripta
Phys. Scr. 90 (2015) 055101 (13pp) doi:10.1088/0031-8949/90/5/055101

Tomographic discord for a system of two coupled nanoelectric circuits

A K Fedorov[1,2], E O Kiktenko[2,3], O V Man'ko[4] and V I Man'ko[4]

[1] Russian Quantum Center, Skolkovo, Moscow 143025, Russia
[2] Bauman Moscow State Technical University, Moscow 105005, Russia
[3] Geoelectromagnetic Research Center of the Schmidt Institute of Physics of the Earth, Russian Academy of Sciences, Troitsk, Moscow Region 142190, Russia
[4] P.N. Lebedev Physical Institute, Russian Academy of Sciences, Moscow 119991, Russia

E-mail: akf@rqc.ru

Received 24 October 2014, revised 6 February 2015
Accepted for publication 12 February 2015
Published 1 April 2015

Abstract

We consider quantum correlations and quantum discord phenomena for two-qubit states with *X*-type density matrices in the tomographic framework of quantum mechanics. By introducing different measurement schemes, we establish the relation between the tomographic approaches to quantum discord, symmetric discord, and measurement-induced disturbance. In our consideration, *X*-states appear as approximations of ground and low temperature thermal states of two coupled harmonic oscillators realized by nanoelectric *LC*-circuits. Possibilities for controlling the amounts of correlations and entropic asymmetry due to variation of the frequency detuning and the coupling constant are also considered.

Keywords: discord, quantum tomography, nanoelectric circuits

(Some figures may appear in colour only in the online journal)

1. Introduction

Inspiring experimental progress on the creation, manipulation, and characterization of individual quantum objects has explored new frontiers in quantum science and technologies [1]. Due to the intriguing properties of quantum systems, they can be viewed as a potential platform for ultra-sensitive metrology [2], unconditionally secure communications [3], highly efficient information processing [4]. and simulation of complex quantum systems [5].

However, the implementation of quantum devices is challenging, because even bipartite quantum systems exhibit a nontrivial behavior and correlation properties. A shining example is that of quantum discord, demonstrating a specific type of quantum correlation in bipartite quantum systems [6–21]. Quantum discord is a measure of quantum correlations based on the subtraction of locally accessible information from the total amount of quantum mutual information. The exploration of quantum discord has inspired a new wave of research on nonlocal properties of separable quantum states [22] and their applications in realizing quantum algorithms [23, 24].

The concept of quantum discord is associated with quantum measurements. A powerful technique for complete experimental characterization of quantum states and processes in terms of nonnegative probability distribution functions is quantum tomography [25]. The tomographic approach was introduced for systems with continuous [26] and discrete variables [27]. Clearly, the tomographic approach generalizes the Shannon information theory on the quantum domain in a very natural way. In the past few decades, a wide class of problems in quantum information theory, e.g. revealing new inequalities for Shannon [28] and Rényi entropies [29–31], the tomographic approach to Bell-type inequalities [32], quantumness tests [33], quantum correlations and quantum discord [31, 34–36], have been investigated in detail [37].

In the quantum optics domain, the field quadratures of an electromagnetic mode play the role of canonical position and momentum operators [38]. Using optical homodyne detection [25, 39, 40], the uncertainty relations, the entropic inequalities and the quantum discord have been experimentally verified [41–43]. It should be noted, however, that the tomographic approach is applicable to arbitrary quantum systems whose

Hilbert space is isomorphic to the Hilbert space of the harmonic oscillator.

Recently, the possibility of applying quantum tomography for the description of quantum states of the current and voltage in a quantum nanoelectric circuit with a Josephson junction has been demonstrated [44, 45]. Using symplectic tomography [26], examples of the Gaussian states of circuits with the Josephson junction and two coupled resonant circuits of high quality have been considered [44]. Tomographic expressions for the Shannon entropy, mutual information, fidelity, and purity of the quantum states of a nanoelectric circuit have been obtained [45].

At the same time, substantial advances in the manufacturing of quantum nanoelectric circuits and superconducting quantum interference devices have been achieved [46]. Due to there being sufficiently low dissipation in nanoelectric circuits, they are promising candidates for providing scalable interfaces between classical circuits and the quantum counterparts [47]. The realization of simple two-qubit algorithms using a superconducting quantum processor has been demonstrated [48].

In addition to their importance in applications [46], nanoelectric circuits and Josephson junctions with time-varying parameters provide useful setups for a model of a parametric quantum oscillator [49–54]. The significance of this model has been shown in theoretical [52–56] and experimental [57] studies of the dynamical Casimir effect [58].

In the present work, we consider quantum correlations, quantum discord, and entropic asymmetry for a class of states with X-type density matrices using quantum tomography. We are interested in several important issues. The class of X-state density matrices considered is of particular interest because there exists an analytical formula for the quantum discord [10–13], which is either precise for a huge subclass of X-states or gives a sufficiently small error [14]. A first important problem is that of revealing the connection between the tomographic approach to quantum discord [31, 34, 35] and discord-related measures [6]. Using various kinds of measurement schemes, we establish the relations among the tomographic discord, symmetric discord based on the von Neumann measurements, and measurement-induced disturbance [9]. Also, we propose an analytical formula for quantum discord as well as examining it for the set of randomly generated two-qubit states. Furthermore, we combine our consideration with quantum causal analysis [59–62], which allows us to reveal significant properties in the entropic asymmetry of states with X-type density matrices [63].

The connection of quantum discord with well-controllable and easily implementable physical systems opens a way to its experimental investigation. There are several notable proposals for realizing quantum states with X-type density matrices for biparticle systems in experiments: spin-1/2 particles with the XY Hamiltonian in the external magnetic field [15]; two-level atoms, driven by a laser field interaction [16]; coupled superconducting circuits, based on Josephson junctions [17]; and others. Recently, it has been demonstrated that two-qubit X-states emerge in the ground states of a large class of Hamiltonians, including the XY model, the XXZ model, and the transverse field Ising model [18]. In view of the aforementioned progress in the manufacturing, characterization and manipulation of superconducting circuits [46–48, 64, 65], we suggest obtaining X-states as approximations of ground and low temperature thermal states for a system of two coupled harmonic oscillators, realized using nanoelectric LC-circuits (figure 1). Thus, the second question concerns the controllability of the amounts of quantum correlations and entropic asymmetry through variation of the frequency detuning and the coupling constant of two coupled nanoelectric LC-circuits. We are also interested in the robustness of correlation properties with respect to the controllable parameters of the physical system and environment.

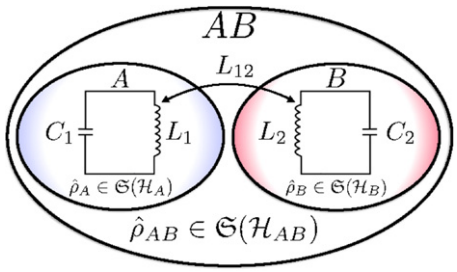

Figure 1. Model of a two-qubit system with an X-type density matrix ρ_{AB}. These states appear as approximations of the ground and low temperature thermal states of two nanoelectric LC-circuits coupled through the mutual inductance L_{12}.

The paper is organized as follows. We review quantum tomography for discrete variables, tomographic information measures, tomographic quantum discord, and causal analysis in section 2. Using various measurement schemes, we establish the connection between tomographic discord and discord-related measures. In section 3, we study various measurement schemes for X-states. Subsequently, we suggest an analytical formula as well as verifying it on the set of randomly generated two-qubit states. X-states are obtained as approximations of ground and low temperature thermal states for two coupled nanoelectric LC-circuits in section 4. We investigate correlation properties of the two-qubit system with an X-type density matrix as a function of the controllable parameters of our physical system: the frequency detuning and the coupling constant of the circuits. Finally, we give the conclusions and prospects in section 5.

2. Quantum tomography

In general, quantum states are described via the density operator $\hat{\rho} \in \mathfrak{S}(\mathcal{H})$, where $\mathfrak{S}(\mathcal{H})$ is the set of positive operators of unit trace $\mathrm{Tr}\,\hat{\rho} = 1$ in a Hilbert space $\mathcal{H}$.

For the finite-dimensional Hilbert space case, we can introduce quantum tomograms as follows:

$$\mathcal{T}(U) = \{\mathcal{T}_m(U)\}\left\{\left\langle m\middle|U\hat{\rho}U^{\dagger}\middle|m\right\rangle\right\}, \tag{1}$$

where $\{|m\rangle\}$ is the complete set of orthonormal vectors, representing a measurement basis, and $U \in \mathrm{SU}(N)$ is the unitary matrix.

Having a fair probability distribution function, quantum tomograms are positive and normalized:

$$\mathcal{T}_m(U) \geqslant 0, \qquad \sum_m \mathcal{T}_m(U) = 1.$$

For qubit systems with $\dim\mathcal{H} = 2$ and $m = |0\rangle, |1\rangle$, the generic form of definition (1) reduces to the SU(2) case [27]. Thus, a matrix $U \in \mathrm{SU}(2)$ can be given in the parameterized form

$$U = U(\theta, \phi) = \begin{pmatrix} \cos\theta/2 & \sin\theta/2 \\ -\sin\theta/2 & \cos\theta/2 \end{pmatrix} \begin{pmatrix} \mathrm{e}^{\mathrm{i}\phi/2} & 0 \\ 0 & \mathrm{e}^{-\mathrm{i}\phi/2} \end{pmatrix}, \quad (2)$$

where θ and ϕ correspond to the Bloch sphere rotation.

2.1. Mutual information

Let us consider a bipartite state AB with the following density operator:

$$\hat{\rho}_{AB} \in \mathfrak{S}\left(\mathcal{H}_{AB} = \mathcal{H}_A \otimes \mathcal{H}_B\right),$$

where the density operators of the subsystems have the forms

$$\hat{\rho}_A = \mathrm{Tr}_B \hat{\rho}_{AB} \in \mathfrak{S}\left(\mathcal{H}_A\right), \quad \hat{\rho}_B = \mathrm{Tr}_A \hat{\rho}_{AB} \in \mathfrak{S}\left(\mathcal{H}_B\right).$$

In quantum information theory, the full amount of correlation between subsystems is measured by the quantum mutual information:

$$I = S_A + S_B - S_{AB}, \quad (3)$$

where S_A, S_B and S_{AB} are the von Neumann entropies, given by the general expression

$$S = -\mathrm{Tr}\left(\hat{\rho}\log\hat{\rho}\right). \quad (4)$$

Here, we take the logarithm to base 2.

In the tomographic picture of quantum mechanics, the bipartite quantum state can be described by a tomogram given in the following form:

$$\mathcal{T}_{AB}\left(U_A \otimes U_B\right) = \left\{\mathcal{T}_{AB_{ij}}\left(U_A \otimes U_B\right)\right\},$$

where U_A and U_B are operators which describe local orthogonal projective measurements on subsystems A and B. Then, the tomograms of the subsystems take the form

$$\mathcal{T}_A\left(U_A\right) = \left\{\mathcal{T}_{A_i}\left(U_A\right)\right\} = \left\{\sum_j \mathcal{T}_{AB_{ij}}\left(U_A \otimes U_B\right)\right\},$$
$$\mathcal{T}_B\left(U_B\right) = \left\{\mathcal{T}_{B_j}\left(U_B\right)\right\} = \left\{\sum_i \mathcal{T}_{AB_{ij}}\left(U_A \otimes U_B\right)\right\}.$$

Being, on the one hand, probability distribution functions, and, on the other hand, applicable for the description of quantum states, quantum tomograms allow us to study both classical and quantum correlations between subsystems in bipartite quantum states.

In this way, we can introduce the tomographic Shannon entropy [28] calculated for the tomogram $\mathcal{T}(U)$:

$$H(U) = -\sum_m \mathcal{T}_m(U)\log\mathcal{T}_m(U). \quad (5)$$

Thus, one can describe the amount of correlation observable via local measurements in the bipartite system AB via the tomographic mutual information:

$$J\left(U_A, U_B\right) = H_A\left(U_A\right) + H_B\left(U_B\right) - H_{AB}\left(U_A \otimes U_B\right), \quad (6)$$

where $H_A(U_A)$, $H_B(U_B)$ and $H_{AB}(U_A \otimes U_B)$ are tomographic Shannon entropies calculated using equation (5) for $\mathcal{T}_A(U_A)$, $\mathcal{T}_B(U_B)$ and $\mathcal{T}_{AB}(U_A \otimes U_B)$, respectively.

Expression (6) shows that the tomographic mutual information is a straightforward analog of (3), while the tomographic Shannon entropy (5) generalizes the von Neumann entropy (4). The value for the tomographic mutual information (6), clearly, depends on operators U_A and U_B.

2.2. The discord

The conventional approach [6] is to define the quantum discord as the difference between the total correlations (3) and the classical correlations obtained after a measurement performed on one subsystem (e.g., on the subsystem B):

$$D^{(B)} = I - \max_{\{\Pi_b\}} J^{(B)}_{\{\Pi_b\}} \geqslant 0, \quad (7)$$

with $J^{(B)}_{\{\Pi_b\}}$ being the quantum mutual information calculated by using Equation (3) for the state

$$\rho^{(B)}_{AB} = \sum_b M_b \rho_{AB} M_b^\dagger, \qquad \Pi_b = M_b^\dagger M_b,$$

where the quantity Π_b introduced is the positive-operator-valued measure (POVM) in the Hilbert space $\mathcal{H}_B$.

On the other hand, from definitions (3) and (6), one can construct the tomographic discord as a tomographic measure of the quantumness of bipartite state correlations:

$$D\left(U_A, U_B\right) = I - J\left(U_A, U_B\right). \quad (8)$$

The tomographic measure (8) resembles the concept of symmetric quantum discord [20]. The difference is as follows. First, in the definition (7) of the quantum discord, a measurement is performed only on one subsystem. Second, the measurement in (8) is described via a set of orthogonal projectors (von Neumann measurements). Finally, there is no maximization procedure in the definition (8).

Due to the dependence of the tomographic mutual information (6) and, therefore, expression (8) on the unitary operators U_A and U_B, the amount of observed correlation (or quantumness) directly depends on the measurements.

We consider three different approaches to the unambiguous definition of such operators.

2.2.1. The optimal measurement scheme. The first approach follows directly from the definition of symmetric quantum discord, related to the von Neumann measurements [21]. The idea is to consider the measurement operators U_A and U_B in

such a way that they maximize the tomographic mutual information (6):

$$\left(U_A^{\rm opt},\, U_B^{\rm opt}\right) = \arg\max_{U_A, U_B} J\left(U_A,\, U_B\right). \tag{9}$$

The resulting tomogram of the state:

$$\mathcal{T}_{AB}^{\rm opt} = \mathcal{T}_{AB}\left(U_A^{\rm opt} \otimes U_B^{\rm opt}\right) \tag{10}$$

makes quantity (8) attain its minimal possible value:

$$D^{\rm opt} = I - J^{\rm opt}, \qquad J^{\rm opt} = J\left(U_A^{\rm opt},\, U_B^{\rm opt}\right). \tag{11}$$

Due to the existence of the maximization procedure in equation (9), we label this approach to the choice of unitary operators U_A and U_B with the corresponding correlation measure as the optimal tomographic discord approach.

2.2.2. The diagonalizing measurement scheme. An alternative natural approach is to consider the unitary operators U_A and U_B in such a way that the density matrices of the subsystem remain undisturbed after the measurement [34]. In other words, the density matrices of the subsystems after the action of the operators become diagonal in the measurement basis.

Applying unitary transformations with these operators to the density matrices of the subsystems, we find that the Shannon entropies of the subsystems become equal to the von Neumann entropies:

$$H_A\left(\widetilde{U}_A^{\rm diag}\right) = S_A, \qquad H_B\left(\widetilde{U}_B^{\rm diag}\right) = S_B.$$

We use the tilde and the superscript 'diag' to identify these operators.

However, there is still ambiguity as regards their choice. For example, for maximally entangled states, the density matrix of the subsystems remains diagonal (and proportional to the identity matrix) under any possible rotation operator.

Therefore, we consider the set of operators given by

$$\left(U_A^{\rm diag},\, U_B^{\rm diag}\right) = \arg\max_{\widetilde{U}_A^{\rm diag}, \widetilde{U}_B^{\rm diag}} J\left(\widetilde{U}_A^{\rm diag},\, \widetilde{U}_B^{\rm diag}\right), \tag{12}$$

not only to make the density matrices of the subsystems diagonal, but also to maximize the level of correlations described by equation (6).

We denote the corresponding tomogram as follows:

$$\mathcal{T}_{AB}^{\rm diag} = \mathcal{T}_{AB}\left(U_A^{\rm diag} \otimes U_B^{\rm diag}\right). \tag{13}$$

As a result, one can introduce the diagonalizing tomographic discord with the following form:

$$D^{\rm diag} = I - J^{\rm diag} = H_{AB}\left(U_A^{\rm diag} \otimes U_B^{\rm diag}\right) - S_{AB},$$
$$J^{\rm diag} = J\left(U_A^{\rm diag},\, U_B^{\rm diag}\right). \tag{14}$$

Introduced in the tomographic framework in [34], this quantity is also well-known as the measurement-induced disturbance [9]. It should be noted that (14) was named the 'tomographic discord' in the work [35]; however, in this work we prefer to use the term 'diagonalizing tomographic discord' because we also consider other approaches, which are inherently tomographic as well.

2.2.3. The symmetrizing measurement scheme. Here, we point out one more auxiliary approach. This approach arises from the fact that for certain classes of states (notably, for *X*-states), it is useful to consider the unitary operators such that tomograms of the subsystems become uniform distributions; e.g., for two-qubit states, the corresponding tomograms read

$$\mathcal{T}_A\left(\widetilde{U}_A^{\rm sym}\right) = \mathcal{T}_B\left(\widetilde{U}_B^{\rm sym}\right) = \{1/2,\, 1/2\}.$$

Consequently, the operators introduced transform the Shannon entropies (see equation (5)) of the subsystems to ones equal to their maximum possible values:

$$H_A\left(\widetilde{U}_A^{\rm sym}\right) = H_B\left(\widetilde{U}_B^{\rm sym}\right) = 1.$$

Like in giving the definitions (10) and (12), we add a requirement that the tomographic mutual information (6) attains its maximum possible value:

$$\left(U_A^{\rm sym},\, U_B^{\rm sym}\right) = \arg\max_{\widetilde{U}_A^{\rm sym}, \widetilde{U}_B^{\rm sym}} J\left(\widetilde{U}_A^{\rm sym},\, \widetilde{U}_B^{\rm sym}\right). \tag{15}$$

Finally, the corresponding measure reads

$$D^{\rm sym} = I - J^{\rm sym} = I + H_{AB}\left(U_A^{\rm sym} \otimes U_B^{\rm sym}\right) - 2,$$
$$J^{\rm sym} = J\left(U_A^{\rm sym} \otimes U_B^{\rm sym}\right). \tag{16}$$

We label this approach as the symmetrizing discord approach.

2.3. Entropic asymmetry

The entropic asymmetry of particular mixed states is another interesting and important issue [63]. Due to such asymmetry, the decoherence acting on different parties leads to different rates of correlation decay. In other words, the question of the robustness of parties appears.

With this in mind, quantum causal analysis [59–62] and its tomographic generalization [35] have been proposed. This approach was successfully implemented for two-qubit [60] and three-qubit [61] states and atom–field interactions [62]. We note that pure bipartite states always have equal von Neumann entropies of the subsystems due to the Schmidt decomposition. In view of this, they are not of interest.

Quantum causal analysis is based on a pair of independence functions [59]:

$$i_{A|B} = \frac{S_A - I}{S_A}, \qquad i_{B|A} = \frac{S_B - I}{S_B},$$

which can be used to provide the measure of the entropic asymmetry:

$$d_{AB} = i_{A|B} - i_{B|A} = I\frac{S_A - S_B}{S_A S_B}. \tag{17}$$

This measure of asymmetry (17) has the following useful properties:

(i) positive values of d_{AB} correspond to a case where the first subsystem plays a decisive role in the correlation as

compared to the second one (in causal analysis, the first subsystem is labeled the 'cause', while the second one is called the 'effect');

(ii) $d_{AB} = -d_{BA}$, i.e., the sign of d_{AB} defines the direction of the asymmetry;

(iii) the magnitude $|d_{AB}|$ corresponds to the extent of the asymmetry of the roles of the subsystems in the correlations.

In turn, the tomographic approach to the amount of asymmetry [35] relies on the tomographic independence functions:

$$i^{\text{tom}}_{A|B}(U_A, U_B) = \frac{H_A(U_A) - J(U_A, U_B)}{H_A(U_A)},$$
$$i^{\text{tom}}_{B|A}(U_A, U_B) = \frac{H_B(U_B) - J(U_A, U_B)}{H_B(U_B)}, \tag{18}$$

with the corresponding measure of asymmetry given in the form

$$d^{\text{tom}}_{AB}(U_A, U_B) = i^{\text{tom}}_{A|B}(U_A, U_B) - i^{\text{tom}}_{B|A}(U_A, U_B). \tag{19}$$

Substituting in (18) the unitary operators U_A and U_B in the forms (9), (12), and (15), we obtain three definite values of the tomographic asymmetry: d^{opt}_{AB}, d^{diag}_{AB} and d^{sym}_{AB}, respectively. However, the third value is of no interest since we always have the identity $d^{\text{sym}}_{AB} = 0$.

Additionally, we note that the diagonalizing scheme has the following important property:

$$\frac{d^{\text{diag}}_{AB}}{d_{AB}} = \frac{J^{\text{diag}}}{I} = 1 - \frac{D^{\text{diag}}}{I} > 0.$$

Thus, this scheme does not change the direction of the original asymmetry, but it can decrease its extent.

3. The tomographic quantum discord for *X*-states

In the current paper, we give our main attention to the class of two-qubit states with *X*-type density matrices:

$$\rho^{X}_{AB} = \begin{pmatrix} \rho_{11} & 0 & 0 & \rho_{14} \\ 0 & \rho_{22} & \rho_{23} & 0 \\ 0 & \rho_{23} & \rho_{33} & 0 \\ \rho_{14} & 0 & 0 & \rho_{44} \end{pmatrix}. \tag{20}$$

The constraints on the elements $\{\rho_{ij}\}$ are the following: (i) all diagonal elements are nonnegative and form a unit trace; (ii) the off-diagonal elements are also nonnegative and their magnitudes are bounded by inequalities:

$$\rho^2_{23} \leqslant \rho_{22}\rho_{33}, \qquad \rho^2_{14} \leqslant \rho_{11}\rho_{44}.$$

We note that any Hermitian matrix in the form (20) with complex off-diagonal elements can always be transformed into an *X*-type matrix with all elements nonnegative by means of a suitable choice of the basis [11].

The *X*-states have paramount importance for the concept of quantum discord [6]. Recently, this class of states has attracted a great deal of interest in the context of a search for an analytical formula for its computation [10–14].

The intention of our work is to study how the optimal (11), diagonalizing (14), and symmetrizing (16) discords relate to each other for the case of *X*-states (20).

3.1. Diagonalizing and symmetrizing tomograms

For *X*-states, tomogram (1) parameterized by the Bloch sphere rotation angles:

$$\mathcal{T}_{AB} = \mathcal{T}_{AB}(\phi_A, \theta_A, \phi_B, \theta_B)$$

can be easily obtained from diagonal elements of the initial density matrix (20) after the application of the rotation operator $U(\phi_A, \theta_A) \bigotimes U(\phi_B, \theta_B)$ (where both operators have the form (2)). The explicit results of our calculations are presented in appendix A.

Here, we consider the main entropic properties:

(i) Due to symmetry considerations, we restrict to studying parameters in the following regions:

$$\theta_A, \theta_B \in [0, \pi/2], \qquad \phi_A, \phi_B \in [0, \pi].$$

(ii) The tomograms of the subsystems appear to be functions only of the rotation angles θ_A and θ_B:

$$\mathcal{T}_A = \mathcal{T}_A(\theta_A), \qquad \mathcal{T}_B = \mathcal{T}_B(\theta_B).$$

Moreover, at $\theta_A = \theta_B = 0$, the tomographic Shannon entropies (5) are equal to the von Neumann ones (4):

$$H_A(\theta_A = 0) = S_A, \qquad H_B(\theta_B = 0) = S_B,$$

whereas for the condition $\theta_A = \theta_B = \pi/2$, they attain their maximum values:

$$H_A(\theta_A = \pi/2) = H_B(\theta_B = \pi/2) = 1.$$

(iii) Since all of the matrix elements in (20) are real, the maximum value of the tomographic mutual information $J(\phi_A, \theta_A, \phi_B, \theta_B)$ at fixed values of the angles θ_A and θ_B is obtained at $\phi_A = \phi_B = 0$.

From (ii) and (iii), it follows directly that the condition $\theta_A = \theta_B = \phi_A = \phi_B = 0$ corresponds to a diagonalizing tomogram with the following form:

$$\mathcal{T}^{\text{diag}}_{AB} = \{\rho_{ii}, i = 1, \ldots, 4\}. \tag{21}$$

Meanwhile, a symmetrizing tomogram is obtained for $\theta_A = \theta_B = \pi/2$ and $\phi_A = \phi_B = 0$, and it has the form

$$\mathcal{T}^{\text{sym}}_{AB} = \left\{\frac{1}{4} + \kappa, \frac{1}{4} - \kappa, \frac{1}{4} - \kappa, \frac{1}{4} + \kappa\right\}, \tag{22}$$

with the parameter $\kappa = (\rho_{14} + \rho_{23})/2$. The explicit formulas (21) and (22) make it straightforward to compute the diagonalizing (14) and symmetrizing (16) discords as well as the corresponding asymmetry measure.

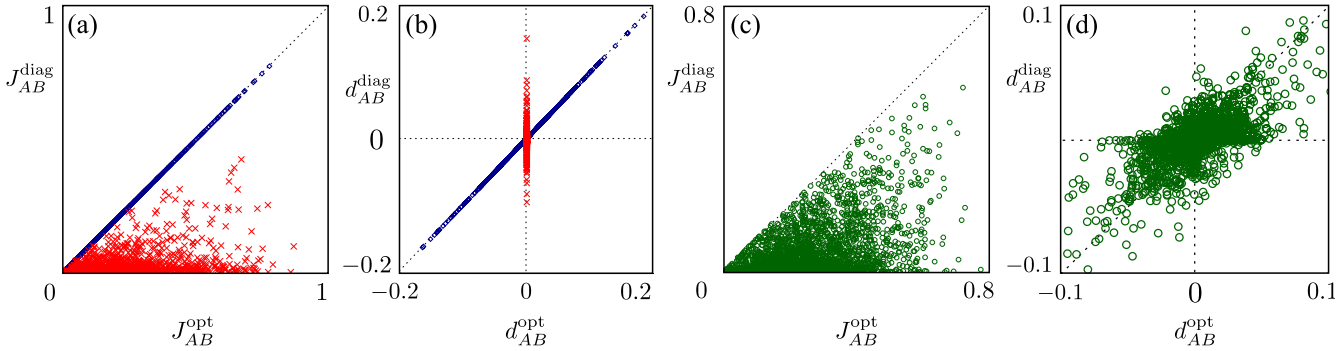

Figure 2. The comparison of the tomographic mutual information (6) and the entropic asymmetry for 3×10^3 randomly generated X-states (see appendix B.1) and 3×10^3 arbitrary mixed two-qubit states (see appendix B.2). In (a) we show a comparison of the tomographic mutual information (6) for X-states obtained from the diagonalizing (14) measurement scheme to that obtained from the optimal (11) measurement scheme. In (b) we show the asymmetry measure obtained from the diagonalizing (14) measurement scheme versus the asymmetry obtained from the optimal (11) measurement scheme. One can see the separation into tomographically asymmetric states (crosses) and tomographically symmetric states (rhombuses). In (c) and (d) the same quantities are shown for randomly generated states (circles).

3.2. The optimal tomogram

To resolve a problem concerning the optimal measurement scheme, we implement a numerical procedure on a set of 3×10^3 randomly generated X-states, similar to that in the work [35]. The methodology used for the generation of random X-states is described in appendix B.1.

The results concerning the comparison between $D^{\rm diag}$ and $D^{\rm opt}$, as well as that between $d_{AB}^{\rm diag}$ and $d_{AB}^{\rm opt}$, are presented in figures 2(a) and (b). Analyzing these numerical results, one can conclude that the class of all X-states generated separates into two subclasses:

(i) the first subclass with (circles in figure 2(a))

$$D^{\rm opt} = D^{\rm diag}, \qquad d^{\rm opt} = d^{\rm diag};$$

(ii) the second subclass with (crosses in figure 2(a))

$$D^{\rm opt} < D^{\rm diag}, \qquad d^{\rm opt} = 0, \qquad \mathcal{T}_{AB}^{\rm opt} = \mathcal{T}_{AB}^{\rm sym}.$$

We conclude that for X-states, the optimal tomogram is either the diagonalizing or the symmetrizing one:

$$D^{\rm opt} = \min\left(D^{\rm diag}, D^{\rm sym}\right). \tag{23}$$

Thus, one can label the first subclass (i) of X-states as the 'tomographically asymmetric' subclass, and the second one (ii) as the 'tomographically symmetric' subclass (see figure 2(b)).

We note that this result is quite in the spirit of the analytical formula for the canonical quantum discord for X-states, obtained in [10], where the optimal measurement for *one* subsystem only should be performed along either the z axis or the x axis of the Bloch sphere (σ_x or σ_z measurements). As has been demonstrated in [12], this approach is not appropriate for all varieties of X-states. In our case, the measurement is performed over *both* subsystems. Then, the established equation (23) seems to be correct for the whole class of states with X-type density matrices. As far as we know, for the two-qubit case the question of whether orthogonal projective measurements, as compared to POVMs of rank 1, maximize the classical correlations is still open.

Besides, pure biparticle quantum states that are not maximally entangled belong to a tomographically asymmetric subclass of the X-states with the optimal measurement basis being defined by their Schmidt decomposition. We note that for maximally entangled states, the diagonalizing and symmetrizing schemes coincide.

Moreover, for pure states the following equalities hold:

$$D^{\rm opt} = D^{\rm diag} = D^{(A)} = D^{(B)} = J^{\rm diag} = \frac{1}{2}I = \mathcal{E}, \tag{24}$$

where $D^{(A)}$ and $D^{(B)}$ are canonical discords (7), obtained from measurements on A and B, respectively; and $\mathcal{E}$ is the entanglement of the formation, just being equal to the entropies S_A=S_B in this case.

In figures 2(c) and (d), we show results obtained for randomly generated arbitrary mixed two-qubit states. The generation of random arbitrary mixed two-qubit states is discussed in appendix B.2.

One can conclude that in the general case the optimal measurement scheme is different both from the diagonalizing one and from the symmetrizing one. Thus, we obtain

$$D^{\rm opt} \leqslant \min\left(D^{\rm diag}, D^{\rm sym}\right).$$

Moreover, the direction of the asymmetry defined by

$$\mathrm{sign}\left(d_{AB}^{\rm diag}\right) = \mathrm{sign}\left(d_{AB}\right)$$

may be opposite to that for $\mathrm{sign}\left(d_{AB}^{\rm opt}\right)$.

Thus, this separation of the subclasses with respect to the correlation measure and measures of the entropic asymmetry introduced is not universal for all two-qubit states (see figure 2(d)), i.e., it is a specific feature of X-states.

4. Ground and thermal states of quantum circuits

In this section, we propose physical realizations for states with X-type density matrices as approximations of ground and low temperature thermal states of coupled quantum nanoelectric circuits (see figure 1).

The Hamiltonian of a system of two circuits with inductances L_1, L_2 and capacitors C_1, C_2, coupled via the mutual inductance L_{12}, reads

$$\hat{\mathcal{H}} = \hat{\mathcal{H}}_1 + \hat{\mathcal{H}}_2 + \hat{V}, \qquad \hat{V} = L_{12}\hat{I}_1\hat{I}_2,$$
$$\left[\hat{I}_i, \hat{Q}_i\right] = \mathrm{i}\hbar\big/L_i, \tag{25}$$

where $\hat{I}$ is the current operator and $\hat{Q}$ is the operator of charge on the plates of a capacitor with the standard commutation relation. Here, the Hamiltonian,

$$\hat{\mathcal{H}}_j = \frac{L_j\hat{I}_j^2}{2} + \frac{\hat{Q}_j^{\,2}}{2C_j}, \qquad j = 1, 2, \tag{26}$$

corresponds to a single resonant circuit.

We assume that the energy of thermal fluctuations in circuits is sufficiently smaller than the energy of quanta, i.e., $\hbar\omega_j > k_{\mathrm{B}}T$, where T is the temperature, $\omega_j = (L_jC_j)^{-1/2}$ is the resonant frequency, and k_{B} is the Boltzmann constant. Thus, we can consider circuits as quantum ones.

Due to the duality between mechanical oscillators and circuits, it is convenient to introduce canonical position and momentum operators:

$$\hat{x}_j = -L_jC_j^{1/2}\hat{I}_j, \quad \hat{p}_j = C_j^{-1/2}\hat{Q}_j,$$
$$\left[\hat{x}_j, \hat{p}_k\right] = \mathrm{i}\hbar\delta_{jk}, \tag{27}$$

where δ_{jk} stands for the Kronecker symbol.

Using (27), we can rewrite the terms of Hamiltonian (25) in the form

$$\hat{\mathcal{H}}_j = \frac{\hat{p}_j^{\,2}}{2} + \frac{\omega_j^2\hat{x}_j^{\,2}}{2}, \qquad \hat{V} = g\omega_1\omega_2\hat{x}_1\hat{x}_2, \tag{28}$$

where $g = L_{12}(L_1L_2)^{-1/2}$ is the dimensionless coupling constant.

One can diagonalize Hamiltonian (25) using the canonical transformation to new canonical variables [67]:

$$\begin{pmatrix}\hat{X}_1\\ \hat{X}_2\end{pmatrix} = M(\Theta)\begin{pmatrix}\hat{x}_1\\ \hat{x}_2\end{pmatrix},$$
$$\begin{pmatrix}\hat{P}_1\\ \hat{P}_2\end{pmatrix} = M(\Theta)\begin{pmatrix}\hat{p}_1\\ \hat{p}_2\end{pmatrix}, \tag{29}$$

where $M(\Theta) = U(\Theta, 0)$ is the rotation operator and

$$\Theta = \arctan\frac{2g\omega_1\omega_2}{\omega_1^2 - \omega_2^2}.$$

As a result, we obtain Hamiltonian (25) in the form of two unit-mass non-interacting oscillators:

$$\hat{\mathcal{H}} = \frac{\hat{P}_1^2}{2} + \frac{\Omega_1^2\hat{X}_1^{\,2}}{2} + \frac{\hat{P}_2^2}{2} + \frac{\Omega_2^2\hat{X}_2^{\,2}}{2}, \tag{30}$$

with new resonant frequencies:

$$\Omega_1^2 = \omega_1^2\cos^2\Theta + \omega_2^2\sin^2\Theta + g\omega_1\omega_2\sin 2\Theta,$$
$$\Omega_2^2 = \omega_1^2\sin^2\Theta + \omega_2^2\cos^2\Theta - g\omega_1\omega_2\sin 2\Theta.$$

As a computational basis for our further consideration, we choose the eigenstates $|m, n\rangle$ of the Hamiltonian $\hat{\mathcal{H}}_1 + \hat{\mathcal{H}}_2$ such that

$$\left(\hat{\mathcal{H}}_1 + \hat{\mathcal{H}}_2\right)|m, n\rangle = E_{m,n}|m, n\rangle, \quad m, n = 0, 1, 2, \ldots,$$

with $E_{m,n} = \hbar\omega_1(m + 1/2) + \hbar\omega_2(n + 1/2)$, where m and n are numbers of energy quanta of the oscillators.

We denote the eigenstates of Hamiltonian (30) with tildes over integers (e.g., $|\tilde{1}, \tilde{2}\rangle$):

$$\left(\hat{\mathcal{H}}_1 + \hat{\mathcal{H}}_2 + \hat{V}\right)|\tilde{m}, \tilde{n}\rangle = E_{\tilde{m},\tilde{n}}|\tilde{m}, \tilde{n}\rangle,$$
$$m, n = 0, 1, 2, \ldots,$$

with $E_{\tilde{m},\tilde{n}} = \hbar\Omega_1(m + 1/2) + \hbar\Omega_2(n + 1/2)$.

We denote the coefficients of decomposition of these states in the computational basis as follows:

$$C_{i,j}^{m,n} = \langle i, j|\,\tilde{m}, \tilde{n}\rangle.$$

One can easily calculate them using the wavefunction of the harmonic oscillator eigenstates:

$$\Psi_l^{(\Omega)}(X) = \frac{\Omega^{1/4}}{\sqrt{\left(2^l l!\right)\sqrt{\pi}}}\exp\left(-\frac{1}{2}\Omega X^2\right)\mathbf{H}_l \times\left(\sqrt{\Omega}X\right), \tag{31}$$

where m is the corresponding quantum number, X is the coordinate, Ω is the frequency, and $\mathbf{H}_l$ stands for the Hermitian polynomial of lth order. Thus, we obtain

$$C_{i,j}^{m,n} = \iint_{-\infty}^{\infty}\mathrm{d}x_1\,\mathrm{d}x_2\,\Psi_i^{(\omega_1)}(x_1)\Psi_j^{(\omega_2)}(x_2) \times\Psi_m^{(\Omega_1)}\left(X_1\right)\Psi_n^{(\Omega_2)}\left(X_2\right). \tag{32}$$

Here, the complex conjugation is omitted because there is no imaginary part in the wavefunctions considered. We note that function (31) is an even function for even m, and it is an odd function otherwise; thus, the parity implies that $C_{i,j}^{m,n} = 0$ for odd $i + j + m + n$.

Further, we consider projections of various states on a two-qubit subspace:

$$\mathcal{H}^{2\mathrm{qb}} = \mathrm{span}\{|0, 0\rangle, |0, 1\rangle, |1, 0\rangle, |1, 1\rangle\},$$

with the projector operator

$$\hat{\Pi}^{2\mathrm{qb}}\colon \mathfrak{S}(\mathcal{H}) \to \mathfrak{S}\left(\mathcal{H}^{2\mathrm{qb}}\right)$$

given in the form

$$\hat{\Pi}^{2\mathrm{qb}} = |0, 0\rangle\langle 0, 0| + |0, 1\rangle\langle 0, 1| + |1, 0\rangle\langle 1, 0| + |1, 1\rangle\langle 1, 1|.$$

Thus, for each state $\hat{\rho}$ we can obtain its two-qubit approximation as follows:

$$\hat{\rho}^{2\mathrm{qb}} = \frac{\hat{\Pi}^{2\mathrm{qb}}\hat{\rho}\hat{\Pi}^{2\mathrm{qb}}}{\mathrm{Tr}\left[\hat{\Pi}^{2\mathrm{qb}}\hat{\rho}\hat{\Pi}^{2\mathrm{qb}}\right]}.$$

The accuracy of the approximation can be estimated with the parameter

$$\alpha = 1 - \mathrm{Tr}\left[\hat{\Pi}^{2\mathrm{qb}}\hat{\rho}\hat{\Pi}^{2\mathrm{qb}}\right] \geqslant 0, \tag{33}$$

which is, obviously, zero for states $\hat{\rho} \in \mathfrak{S}(\mathcal{H}^{2\mathrm{qb}})$.

4.1. The ground state

The ground state of Hamiltonian (30) has the simple form $|\psi_{\mathrm{gr}}\rangle = |\tilde{0}, \tilde{0}\rangle$. Due to the parity, its projection on the subspace $\mathcal{H}^{2\mathrm{qb}}$ consists of only two terms:

$$\hat{\Pi}^{2\mathrm{qb}}\,|\tilde{0}, \tilde{0}\rangle = C_{00}^{00}\,|0, 0\rangle + C_{11}^{00}\,|1, 1\rangle. \tag{34}$$

Then, the two-qubit approximation of the state $\hat{\rho}_{\mathrm{gr}} = |\psi_{\mathrm{gr}}\rangle\langle\psi_{\mathrm{gr}}|$ reads

$$\hat{\rho}_{\mathrm{gr}}^{2\mathrm{qb}} = \frac{1}{\left(C_{00}^{00}\right)^2 + \left(C_{11}^{00}\right)^2} \times \begin{pmatrix} \left(C_{00}^{00}\right)^2 & 0 & 0 & C_{00}^{00}C_{11}^{00} \\ 0 & 0 & 0 & 0 \\ 0 & 0 & 0 & 0 \\ C_{00}^{00}C_{11}^{00} & 0 & 0 & \left(C_{11}^{00}\right)^2 \end{pmatrix}, \tag{35}$$

with the accuracy parameter (33) in the form

$$\alpha = 1 - \left(C_{00}^{00}\right)^2 - \left(C_{11}^{00}\right)^2. \tag{36}$$

Like all pure states, the (35) state belongs to the class of X-states.

4.2. The thermal state

The second state that we are interested in is a thermal state. It is given by the general expression

$$\hat{\rho}_{\mathrm{th}} = \frac{1}{Z}\exp\left(-\frac{\hat{\mathcal{H}}}{k_{\mathrm{B}}T}\right),$$
$$Z = \mathrm{Tr}\left[\exp\left(-\frac{\hat{\mathcal{H}}}{k_{\mathrm{B}}T}\right)\right],$$

where $\hat{\mathcal{H}}$ is the Hamiltonian (30), and Z is the partition function. More explicitly, the density operator can be written in the following form:

$$\hat{\rho}_{\mathrm{th}} = \frac{1}{Z}\sum_{m,n\geqslant 0}\left[\exp\left(-\frac{E_{\tilde{m},\tilde{n}}}{k_{\mathrm{B}}T}\right)|\tilde{m}, \tilde{n}\rangle\langle\tilde{m}, \tilde{n}|\right]. \tag{37}$$

We assume that the temperature T is low enough for us to consider the final number of terms in (37) in a such way that the total number of quanta in each term is not greater than 2. Again, we use projections on the subspace $\mathcal{H}^{2\mathrm{qb}}$. The final form of the state (37) considered reads

$$\hat{\rho}_{\mathrm{th}}^{2\mathrm{qb}} = \frac{1}{Z_1}\hat{W}, \qquad Z_1 = \mathrm{Tr}\left[\hat{W}\right], \tag{38}$$

where the operator $\hat{W}$ has the form

$$\hat{W} = \hat{\Pi}^{2\mathrm{qb}} \sum_{\substack{m,n\geqslant 0,\\ m+n\leqslant 2}} \times \left[\exp\left(-\frac{E_{\tilde{m},\tilde{n}}}{k_{\mathrm{B}}T}\right)|\tilde{m}, \tilde{n}\rangle\langle\tilde{m}, \tilde{n}|\right]\hat{\Pi}^{2\mathrm{qb}}.$$

In this case, the accuracy parameter (33) is given by

$$\alpha = 1 - \frac{Z_1}{Z}. \tag{39}$$

From the parity, it follows that the nonzero projections of the vectors used in (37) are given by (see also (34))

$$\hat{\Pi}^{2\mathrm{qb}}\,|\tilde{0}, \tilde{1}\rangle = C_{01}^{01}\,|0, 1\rangle + C_{10}^{01}\,|1, 0\rangle,$$
$$\hat{\Pi}^{2\mathrm{qb}}\,|\tilde{1}, \tilde{0}\rangle = C_{01}^{10}\,|0, 1\rangle + C_{10}^{10}\,|1, 0\rangle,$$
$$\hat{\Pi}^{2\mathrm{qb}}\,|\tilde{1}, \tilde{1}\rangle = C_{00}^{11}\,|0, 0\rangle + C_{11}^{11}\,|1, 1\rangle,$$
$$\hat{\Pi}^{2\mathrm{qb}}\,|\tilde{0}, \tilde{2}\rangle = C_{00}^{02}\,|0, 0\rangle + C_{11}^{02}\,|1, 1\rangle,$$
$$\hat{\Pi}^{2\mathrm{qb}}\,|\tilde{2}, \tilde{0}\rangle = C_{00}^{20}\,|0, 0\rangle + C_{11}^{20}\,|1, 1\rangle.$$

This fact implies that the state $\hat{\rho}_{\mathrm{th}}^{2\mathrm{qb}}$ (37) is an X-state.

4.3. The quantum discord for two coupled circuits

In this part, we consider different measures of correlations for X-states, realized in two-qubit approximations of the ground (35) and thermal states (38) of two coupled oscillators. The measures of correlations considered are:

(i) the quantum mutual information (3);
(ii) the diagonalizing discord D^{diag} (14);
(iii) the symmetrizing discord D^{sym} (16);
(iv) the canonical quantum discords $D^{(A)}$ and $D^{(B)}$ obtained in the form (7) with measurements on the subsystems A and B, respectively;
(iv) the entanglement of formation $\mathcal{E}$.

We compute the latter using the concurrence $\mathcal{C}$ via a general formula [66]:

$$\mathcal{E} = h\left(\frac{1}{2} + \frac{1}{2}\sqrt{1 - \mathcal{C}^2}\right),$$

where $h(x) = -x\log x - (1 - x)\log(1 - x)$ is the binary entropy function. In turn, the concurrence $\mathcal{C}$ for the two-qubit density matrix ρ_{AB} is given by

$$\mathcal{C} = \max\left(0, \lambda_1 - \lambda_2 - \lambda_3 - \lambda_4\right),$$

where the λ_i are written in terms of the eigenvalues of the following matrix in descending order:

$$R = \sqrt{\sqrt{\rho}\left(\sigma_y \otimes \sigma_y\right)\rho^*\left(\sigma_y \otimes \sigma_y\right)\sqrt{\rho}}\,.$$

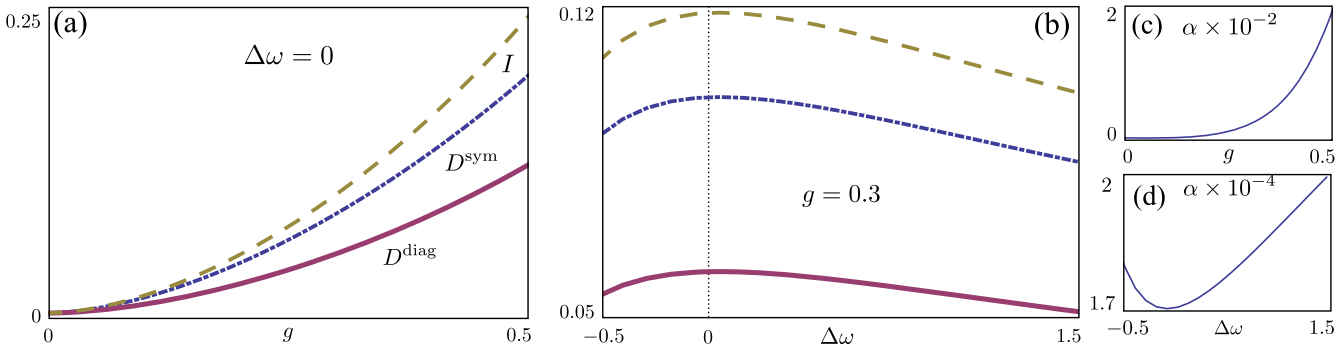

Figure 3. Measures of correlations in the two-qubit approximation of the ground state (35): the quantum mutual information I (dashed), symmetric discord $D^{\rm sym}$ (dot–dashed), and diagonalizing discord $D^{\rm diag}$ (solid). In (a) we show the measures of the correlations as functions of the coupling parameter g at the detuning $\Delta\omega = 0$; in (b) we show the same measures as functions of the detuning $\Delta\omega$ at the fixed coupling constant $g = 0.3$. The validities of the two-qubit approximation estimated with the parameter α (36) are shown in (c) and (d), respectively. For the state (35) considered, the diagonalizing discord $D^{\rm diag}$ is equal to the entanglement of formation $\mathcal{E}$ and the optimal discord $D^{\rm opt}$ (see equation (24)).

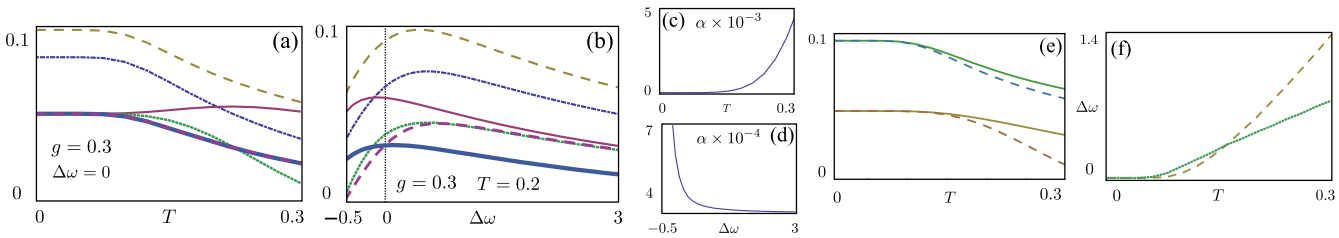

Figure 4. Measures of correlations in the two-qubit approximation of the thermal state (38): the quantum mutual information I (dashed), symmetric discord $D^{\rm sym}$ (dot–dashed), diagonalizing discord $D^{\rm diag}$ (solid), canonical discord $D^{(A)}$ (bold solid), canonical discord $D^{(B)}$ (bold dashed), and entanglement of formation $\mathcal{E}$ (dotted). In (a) we show the measures of the correlations as functions of the temperature T at the resonance $\Delta\omega = 0$ and the coupling constant $g = 0.3$. In (b) we show the measures of the correlations as functions of the detuning $\Delta\omega$ at the coupling constant $g = 0.3$ and the temperature $T = 0.2$. The validities of the two-qubit approximation estimated with parameter α given by (39) are shown in (c) and (d), respectively. In (e) we show the maximum possible values of I and $\mathcal{E}$ accessible at a given temperature and the coupling constant $g = 0.3$ (solid lines), compared with the corresponding values (dashed lines) at the resonance $\Delta\omega = 0$. In (f) we show the values of the detuning $\Delta\omega$, which correspond to the maximum values of the quantum mutual information I (dashed) and the entanglement of formation $\mathcal{E}$ (dotted).

Here, a star stands for complex conjugation, and σ_y for the corresponding Pauli matrix.

We use dimensionless variables, assuming that $\hbar = k_{\rm B} = 1$. Without loss of generality, the frequency ω_1 of the first circuit is assumed to be 1, and we express the second one via the detuning $\Delta\omega$: $\omega_2 = \omega_1 + \Delta\omega$. We consider two types of detuning: the blue detuning ($\Delta\omega > 0$) and the red detuning ($\Delta\omega < 0$).

We note that the optimal discord $D^{\rm opt}$ is the minimum of the values $D^{\rm diag}$ and $D^{\rm sym}$ (see (23)). In addition, to reveal the extent to which our two-qubit approximation remains appropriate, we compute the accuracy parameters (33) and (39).

4.3.1. The ground state. We start with investigation of the two-qubit approximation of the ground state (35). First, for the resonance case ($\Delta\omega = 0$) and different values of the coupling constant g, the results obtained are presented in figures 3(a). We see that all measures of correlations grow with the coupling constant g. As for all pure states (see (24)), the tomographic discord calculated in the diagonalizing scheme $D^{\rm diag}$ appears to be optimal ($D^{\rm opt} = D^{\rm diag}$), and it coincides with the canonical discords $D^{(A)}$ and $D^{(B)}$ as well as with the entanglement of formation $\mathcal{E}$. As state (35) is not maximally entangled, the symmetric discord $D^{\rm sym}$ is invariably greater than the diagonal discord $D^{\rm diag}$. In other words, equality (24)holds.

Second, figure 3(b) shows the influence of detuning at fixed value of the coupling constant ($g = 0.3$). The level of the correlations decreases, but to a rather small extent. As for all states that are not maximally entangled, the equality $D^{\rm opt} = D^{\rm diag}$ holds.

The validities of the two-qubit approximation estimated with parameter (36) are presented in figures 3(c) and (d). We note that the variation of the accuracy parameter α (36) for detuning $\Delta\omega \neq 0$ is sufficiently small.

4.3.2. The thermal state. Here, we study the measures of the correlations in the two-qubit approximation for the thermal state (37).

First, for the resonance case ($\Delta\omega = 0$) and the coupling constant $g = 0.3$, the results for the measures of the correlations as functions of the temperature are presented in figure 4(a). We note that in the resonant case, the two

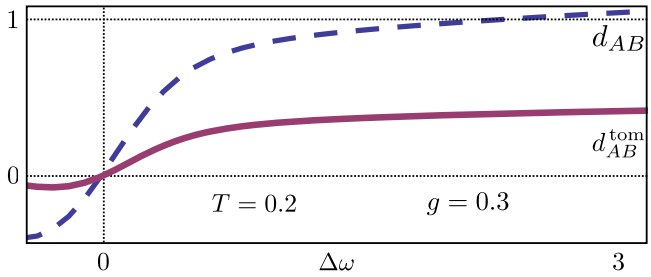

Figure 5. Quantum (17) and tomographic (19) measures of the entropic asymmetry for the thermal state (37).

canonical discords (7) are equal ($D^{(A)} = D^{(B)}$). Furthermore, at the temperature $T \lesssim 0.1$, they are very close to two other correlation measures: $D^{\mathrm{opt}} = D^{\mathrm{diag}}$ and $\mathcal{E}$. At the temperature $T \gtrsim 0.1$, the diagonalizing discord D^{diag} becomes an inappropriate measure of quantum correlations; and at $T \gtrsim 0.22$, the optimal measurement scheme changes from the diagonalizing one to the symmetrizing one. At higher temperatures, the value of $D^{\mathrm{opt}} = D^{\mathrm{sym}}$ naturally decays, like all other measures.

Second, for the fixed temperature $T = 0.3$ and the coupling constant $g = 0.3$, the influence of the detuning $\Delta\omega$ is depicted in figure 4(b). We see that with the presence of detuning, the equality of the canonical discords fails. Thus, we conclude the following:

$$D^{(A)} > D^{(B)}, \qquad \text{for } \Delta\omega < 0;$$
$$D^{(B)} > D^{(A)}, \qquad \text{for } \Delta\omega > 0.$$

Also, one might mention that the maxima of the correlations measured via I and $\mathcal{E}$ have shifted to the area with $\Delta\omega > 0$. Notably, these maxima correspond to slightly different values of the detuning. The validities of the two-qubit approximation estimated with parameter α given by (39) are shown in (c) and (d).

In figure 4(e), for the given temperature $T = 0.2$ and the coupling constant $g = 0.3$, we show the maximum possible values of I and $\mathcal{E}$ and how they compare to the corresponding values obtained at resonance. One can see that the difference for $\mathcal{E}$ is rather dramatic. In figure 4(f), we show the behaviors of the detuning, which give corresponding maximum values of the correlation measures. At high temperature, they have different asymptotic behaviors. However, the validity of our two-qubit approximation fails; therefore this dependence is not of interest. As was to be expected, the two-qubit approximation validity measured with α decreases with growth of the temperature.

Finally, we consider the entropic asymmetry of the thermal state (37) at finite temperature as a function of the detuning. For the temperature $T = 0.2$ and the coupling parameter $g = 0.3$, the results obtained are shown in figure 5. One can see that the entropic asymmetry measured by d_{AB} (17) and d_{AB}^{tom} (19) changes its direction *exactly* at the resonance. Furthermore, the behavior is similar to that of the asymmetry between the discords $D^{(A)}$ and $D^{(B)}$. The oscillator with higher frequency (that is, B at $\Delta\omega > 0$ and A at $\Delta\omega < 0$) always turns out to be an 'effect' with respect to another oscillator. In a mechanical analogy, lower frequency corresponds to higher mass (if we assume that the stiffness coefficients are equal). Thus, one can conclude that in thermal states the heavier oscillator, obviously, plays a more important role than the lighter one.

Moreover, from the comparison with the corresponding behaviors of the discords $D^{(A)}$ and $D^{(B)}$, we conclude that the measurement made on the 'cause' gives us more access to correlations than the measurement on the 'effect'. Speaking in the framework of quantum causal analysis, we have $D^{(\text{'cause'})} < D^{(\text{'effect'})}$. At the same time, with the growth of asymmetry measured with d_{AB}, the discord obtained by measurement of the 'effect' tends to the optimal one.

It is interesting that at high blue detuning ($\Delta\omega > 0$), d_{AB} becomes larger than unity, which is in principle possible only for quantum systems (for classical systems, the highest asymmetry $|d_{AB}| = 1$ is obtained when one of the independence functions is equal to zero, while the other tends to unity). On the other hand, the tomographic measure d_{AB}^{tom} does not demonstrate such a high level of asymmetry in this state.

5. Conclusion and outlook

In conclusion, we point out the main results of the present paper. We have considered a tomographic approach to quantum discord and marked out three particular measurement schemes: the optimal (11), diagonalizing (14), and symmetrizing (16) ones. We have established the explicit relation between the tomographic discord, the symmetric discord based on von Neumann measurements, and the measurement-induced disturbance [9]. More precisely, in the general case, the optimal discord coincides with the symmetric discord, while the diagonalizing discord is equal to the measurement-induced disturbance.

We have focused our attention on X-states and have obtained that their optimal discord amounts either to the diagonalizing discord or to the symmetrizing discord, which implies the analytical formula (23) for its calculation. Combining these results with quantum causal analysis allows us to separate X-states into 'tomographically asymmetric' and 'tomographically symmetric' subclasses (figure 2(b)). Numerical results with randomly generated arbitrary mixed states have shown that this separation is a feature of X-states.

We have considered two-qubit X-states that appear as approximations of the ground (35) and low temperature thermal states (37) of two coupled nanoelectric LC-circuits. We have discussed the robustness of the correlation properties with respect to the environmental parameters, and have shown that for the thermal state (37), blue detuning of the second circuit can raise the amount of correlation as compared to the resonance case.

Also, we have obtained that X-states appearing in coupled circuits mostly belong to the 'tomographically asymmetric' subclass, although variation of the parameters (temperature or detuning) can transform the subclass of the X-state from asymmetrical to symmetrical. This change is

always in the direction in which the two-qubit approximation becomes inappropriate.

We have shown that the behavior of the entropic asymmetry, as observed by quantum causal analysis, conforms with the behavior of the asymmetry between the canonical discords obtained by measurement on different subsystems. In this way, it has been found that a measurement performed on a qubit classified by causal analysis as a 'cause' gives access to more correlations than a measurement performed on the 'effect'.

We expect the presentation of the results in the framework of a real physical system of two coupled nanoelectric circuits to open the way to experimental study of tomographic quantum discord phenomena.

Acknowledgments

We thank S N Filippov and Y V Kurochkin for useful discussions, and Y Huang for insightful comments. This work was supported by the Dynasty Foundation, the Council for Grants of the President of the Russian Federation (grant SP-961.2013.5, E.O.K.), and the Russian Foundation for Basic Research (grant 14-08-00606).

Appendix A. The tomography of *X*-states

To obtain the explicit form of the tomogram for the X-state density matrix (20), one needs to take the diagonal elements of the matrix:

$$\tilde{\rho} = U\left(\phi_A, \theta_A\right) \otimes U\left(\phi_B, \theta_B\right) \times \rho_{AB}^{X} U^{\dagger}\left(\phi_A, \theta_A\right) \otimes U^{\dagger}\left(\phi_B, \theta_B\right).$$

In this way, we obtain the following representation for the tomogram:

$$\mathcal{T}_{AB} = \begin{Bmatrix} \frac{1}{4} + \frac{1}{4} z_A \cos\theta_A + \frac{1}{4} z_B \cos\theta_B + \frac{1}{4} z_{AB} \cos\theta_A \cos\theta_B + \frac{1}{2} \sin\theta_A \sin\theta_B \left(\rho_{14} \cos\left(\phi_A + \phi_B\right) + \rho_{23} \cos\left(\phi_A - \phi_B\right)\right) \\ \frac{1}{4} + \frac{1}{4} z_A \cos\theta_A - \frac{1}{4} z_B \cos\theta_B - \frac{1}{4} z_{AB} \cos\theta_A \cos\theta_B - \frac{1}{2} \sin\theta_A \sin\theta_B \left(\rho_{14} \cos\left(\phi_A + \phi_B\right) + \rho_{23} \cos\left(\phi_A - \phi_B\right)\right) \\ \frac{1}{4} - \frac{1}{4} z_A \cos\theta_A + \frac{1}{4} z_B \cos\theta_B - \frac{1}{4} z_{AB} \cos\theta_A \cos\theta_B - \frac{1}{2} \sin\theta_A \sin\theta_B \left(\rho_{14} \cos\left(\phi_A + \phi_B\right) + \rho_{23} \cos\left(\phi_A - \phi_B\right)\right) \\ \frac{1}{4} - \frac{1}{4} z_A \cos\theta_A - \frac{1}{4} z_B \cos\theta_B + \frac{1}{4} z_{AB} \cos\theta_A \cos\theta_B + \frac{1}{2} \sin\theta_A \sin\theta_B \left(\rho_{14} \cos\left(\phi_A + \phi_B\right) + \rho_{23} \cos\left(\phi_A - \phi_B\right)\right) \end{Bmatrix},$$

where we use the notation

$$z_A = \rho_{11} + \rho_{22} - \rho_{33} - \rho_{44},$$
$$z_B = \rho_{11} - \rho_{22} + \rho_{33} - \rho_{44},$$
$$z_{AB} = \rho_{11} - \rho_{22} - \rho_{33} + \rho_{44}.$$

The order of elements in the tomogram is governed by the rules of standard tensor multiplication:

$$\mathcal{T}_{AB} = \left\{\mathcal{T}_{AB_{00}}, \mathcal{T}_{AB_{01}}, \mathcal{T}_{AB_{10}}, \mathcal{T}_{AB_{11}}\right\}.$$

The reduced tomogram takes the simple form

$$\mathcal{T}_A = \left\{\frac{1}{2} + \frac{1}{2} z_A \cos\theta_A, \frac{1}{2} - \frac{1}{2} z_A \cos\theta_A\right\},$$
$$\mathcal{T}_B = \left\{\frac{1}{2} + \frac{1}{2} z_B \cos\theta_B, \frac{1}{2} - \frac{1}{2} z_B \cos\theta_B\right\},$$

without the dependences on ϕ_A and ϕ_B.

Appendix B. The generation of random two-qubit states

B.1. The generation of random X-states

To generate the X-state density matrix (20), we use the following algorithm. First, we generate the diagonal elements as follows:

$$\rho_{ii} = \frac{p_i}{\sum_{j=1}^{4} p_j}, \qquad p_i = \mathcal{U}(0, 1),$$

where $\mathcal{U}(a, b)$ stands for a uniform distribution on $[a, b]$.

Then we generate off-diagonal elements as follows:

$$\rho_{14} = \epsilon_1 \sqrt{\rho_{11}\rho_{44}}, \qquad \rho_{23} = \epsilon_2 \sqrt{\rho_{22}\rho_{33}},$$
$$\epsilon_1, \epsilon_2 = \mathcal{U}(0, 1).$$

We note that this rather straightforward algorithm does not generate states uniformly with respect to the Haar measure, so it is quite useful for observing two possible subclasses of X-states but is not appropriate for a study of the relative volumes of each of the subclasses in the whole set of X-states.

B.2. The generation of random arbitrary two-qubit mixed states

We generate arbitrary two-qubit states using the following form:

$$\rho_{AB} = \frac{1}{\sum_{j=1}^{4} p_j} \sum_{k=1}^{4} p_k \left\langle \psi_k \middle| \psi_k \right\rangle^{-1} \left| \psi_k \right\rangle \left\langle \psi_k \right|,$$

where

$$\left|\psi_k\right\rangle = \begin{pmatrix} \mathcal{N}(0,1) \\ \mathcal{N}(0,1) \\ \mathcal{N}(0,1) \\ \mathcal{N}(0,1) \end{pmatrix} + \mathrm{i} \begin{pmatrix} \mathcal{N}(0,1) \\ \mathcal{N}(0,1) \\ \mathcal{N}(0,1) \\ \mathcal{N}(0,1) \end{pmatrix}, \qquad p_j = \mathcal{U}(0,1),$$

with $\mathrm{i}^2 = -1$, and $\mathcal{N}(\mu, \sigma)$ being the Gaussian distribution with the expectation value μ and the standard deviation σ. According to [68], this method gives a uniform distribution of quantum states.

References

[1] Thompson J and Lukin M D 2014 *Science* **345** 272
[2] Ye J, Kimble H J and Katori H 2008 *Science* **320** 1734
[3] Gisin N, Ribordy G, Tittel W and Zbinden H 2002 *Rev. Mod. Phys.* **74** 145
[4] Ladd T D, Jelezko F, Laflamme R, Nakamura Y, Monroe C and O'Brien J L 2010 *Nature* **464** 45
[5] Cirac J I and Zoller P 2012 *Nature Phys.* **8** 264
[6] For a review, see Modi K, Brodutch A, Cable H, Paterek T and Vedral V 2012 *Rev. Mod. Phys.* **84** 1655
[7] Zurek W H 2000 *Ann. Phys.* **9** 855
Ollivier H and Zurek W H 2001 *Phys. Rev. Lett.* **88** 017901
[8] Henderson L and Vedral V 2001 *J. Phys. A: Math. Gen.* **34** 6899
[9] Luo S 2008 *Phys. Rev.* A **77** 042303
[10] Ali M, Rau A R P and Alber G 2010 *Phys. Rev.* A **81** 042105
Ali M, Rau A R P and Alber G 2010 *Phys. Rev.* A **82** 069902
[11] See also Fanchini F F, Werlang T, Brasil C A, Arruda L G E and Caldeira A O 2010 *Phys. Rev.* A **81** 052107
[12] See also the recent study of Maldonado-Trapp A, Hu A and Roa L 2015 *Quantum Inf. Process.* doi:10.1007/s11128-015-0943-y
[13] The formula has been established by Chen Q, Zhang C, Yu S, Yi X X and Oh C H 2011 *Phys. Rev.* A **84** 042313 with the use of the POVM in the definition of the quantum discord and by
Huang Y 2013 *Phys. Rev.* A **88** 014302 for the case of von Neumann measurements.
[14] Namkung M, Chang J, Shin J and Kwon Y 2015 *Int. J. Theor. Phys.* doi:10.1007/s10773-015-2573-7
[15] Fel'dman E B and Zenchuk A I 2011 *JETP Lett.* **93** 459
[16] Castanõs L O 2012 *Phys. Rev.* A **85** 062103
[17] Yu Y, Fu G, Guo L P, Pan H and Wang Z S 2013 *Physica* C **495** 88
[18] Huang Y 2014 *Phys. Rev.* B **89** 054410
[19] Chernyavskiy A Y, Doronin S I and Fel'dman E B 2014 *Phys. Scr.* T **160** 014007
[20] Luo S and Zhang Q 2009 *J. Stat. Phys* **136** 165
Maziero J, Céleri L C and Serra R M arXiv:1004.2082
[21] Girolami D, Paternostro M and Adesso G 2011 *J. Phys. A: Math. Theor.* **44** 352002
[22] Horodecki M, Horodecki P, Horodecki R, Oppenheim J, Sen A, Sen U and Synak-Radtke B 2005 *Phys. Rev.* A **71** 062307
Niset J and Cerf N J 2006 *Phys. Rev.* A **74** 052103
[23] Lanyon B P, Barbieri M, Almeida M P and White A G 2008 *Phys. Rev. Lett.* **101** 200501
[24] See also Bennett C H, DiVincenzo D P, Fuchs C A, Mor T, Rains E, Shor P W, Smolin J A and Wootters W K 1999 *Phys. Rev.* A **59** 1070
Braunstein S L, Caves C M, Jozsa R, Linden N, Popescu S and Schack R 1999 *Phys. Rev. Lett.* **83** 1054
Meyer D A 2000 *Phys. Rev. Lett.* **85** 2014
[25] For a review, see Lvovsky A I and Raymer M G 2009 *Rev. Mod. Phys.* **81** 299
[26] Mancini S, Man'ko V I and Tombesi P 1995 *Quantum Semiclass. Opt.* **7** 615
Mancini S, Man'ko V I and Tombesi P 1996 *Phys. Lett. A* **213** 1
D'Ariano G M, Mancini S, Man'ko V I and Tombesi P 1995 *Quantum Semiclass. Opt.* **7** 615
Man'ko O V and Man'ko V I 1997 *J. Russ. Laser Res.* **18** 407
[27] Man'ko V I and Man'ko O V 1997 *J. Exp. Theor. Phys.* **85** 430
Dodonov V V and Man'ko V I 1997 *Phys. Lett.* A **229** 335
Man'ko V I, Man'ko O V and Safonov S S 1998 *Theor. Math. Phys.* **115** 520
Filippov S N and Man'ko V I 2008 *J. Russ. Laser Res.* **29** 564
Russ J 2013 *Laser Res.* **34** 14
Fedorov A K and Kiktenko E O 2013 *J. Russ. Laser Res.* **34** 477
[28] Man'ko O V and Man'ko V I 2004 *J. Russ. Laser Res.* **25** 115
de Nicola S, Fedele R, Man'ko M A and Man'ko V I 2007 *Theor. Math. Phys.* **152** 1081
[29] Man'ko M A, Man'ko V I and Mendes R V 2006 *J. Russ. Laser Res.* **27** 507
[30] Fedorov A K, Kiktenko E O, Man'ko O V and Man'ko V I arXiv:1411.0157
[31] Man'ko M A and Man'ko V I 2013 *J. Russ. Laser Res.* **34** 203
[32] Mancini S, Man'ko V I, Shchukin E V and Tombesi P 2003 *J. Opt. B: Quantum Semiclass.* **5** S333
Lupo C, Man'ko V I and Marmo G 2006 *J. Phys. A: Math. Gen.* **39** 12515
Lupo C, Man'ko V I and Marmo G 2007 *J. Phys. A: Math. Theor.* **40** 13091
Andreev V A, Man'ko V I, Man'ko O V and Shchukin E V 2006 *Theor. Math. Phys.* **146** 140
Filippov S N and Man'ko V I 2009 *J. Russ. Laser Res.* **30** 55
[33] Filippov S N and Man'ko V I 2009 *J. Russ. Laser Res.* **30** 443
Filippov S N and Man'ko V I 2009 *Phys. Scr.* **79** 055007
[34] Man'ko V I and Yurkevich A 2013 *J. Russ. Laser Res.* **34** 463
[35] Kiktenko E O and Fedorov A K 2014 *Phys. Lett.* A **378** 1704
[36] Manko O V and Chernega V N 2013 *JETP Lett.* **97** 557
[37] For a review, see Ibort A, Man'ko V I, Marmo G, Simoni A and Ventriglia F 2009 *Phys. Scr.* **79** 065013
[38] Leonhardt U 1997 *Measuring the Quantum State of Light* (Cambridge: Cambridge University Press)
[39] Smithey D T, Beck M, Raymer M G and Faridani A 1993 *Phys. Rev. Lett.* **70** 1244
[40] Beck M, Smithey D T and Raymer M G 1993 *Phys. Rev.* A **48** R890
Smithey D T, Beck M, Cooper J, Raymer M G and Faridani A 1993 *Phys. Scr.* **48** 35
[41] Man'ko V I, Marmo G, Porzio A, Solimeno S and Ventriglia F 2011 *Phys. Scr.* **83** 045001
[42] Bellini M, Coelho A S, Filippov S N, Man'ko V I and Zavatta A 2012 *Phys. Rev.* A **85** 052129
[43] Hosseini S, Rahimi-Keshari S, Haw J Y, Assad S M, Chrzanowski H M, Janousek J, Symul T, Ralph T C and Lam P K 2014 *J. Phys. B: At. Mol. Opt. Phys.* **47** 025503
[44] Man'ko O V 2012 *AIP Conf. Proc.* **1424** 221
[45] Man'ko O V 2013 *Phys. Scr.* T **153** 014046
[46] For a review, see Maklin Y, Schön G and Schnirman A 2001 *Rev. Mod. Phys.* **73** 357
Clarke J and Wilhelm F K 2008 *Nature* **453** 1031
[47] Blais A, Huang R-S, Wallraff A, Girvin S M and Schoelkopf R J 2004 *Phys. Rev.* A **69** 062320
Las Heras U, Mezzacapo A, Lamata L, Filipp S, Wallraff A and Solano E 2014 *Phys. Rev. Lett.* **112** 200501
Fedorov K G, Shcherbakova A V, Wolf M J, Beckmann D and Ustinov A V 2014 *Phys. Rev. Lett.* **112** 160502
[48] DiCarlo L *et al* 2009 *Nature* **460** 240
Lucero E *et al* 2012 *Nature Phys.* **8** 719

[49] Dodonov V V, Man'ko V I and Man'ko O V 1989 *J. Sov. Laser Res.* **10** 413
Dodonov V V, Man'ko V I and Man'ko O V 1990 *Meas. Technol.* **33** 102
Dodonov V V, Man'ko V I and Man'ko O V 1992 *J. Sov. Laser Res.* **13** 196
Dodonov V V, Man'ko V I and Man'ko O V 1991 *Proc. Lebedev Phys. Inst* **200** 155
Dodonov V V, Man'ko V I and Man'ko O V 1993 *Proc. Lebedev Phys. Inst* **205** 217
[50] Man'ko V I 1991 *J. Sov. Laser Res.* **12** 383
[51] Man'ko O V 1994 *J. Korean Phys. Soc.* **27** 1
[52] Dodonov V V 2001 *Adv. Chem. Phys.* **119** 309
Dodonov V V 2010 *Phys. Scr.* **82** 038105
[53] Dodonov A V, Dodonov E V and Dodonov V V 2003 *Phys. Lett.* A **317** 378
[54] Dodonov V V and Dodonov A V 2005 *J. Russ. Laser Res.* **26** 445
[55] Dodonov V V, Klimov A B and Nikonov D E 1993 *Phys. Rev.* A **47** 4422
Lozovik Y E, Tsvetus V G and Vinogradov E A 1995 *JETP Lett.* **61** 723
[56] Takashima K, Hatakenaka N, Kurihara S and Zeilinger A 2008 *J. Phys. A: Math. Theor.* **41** 164036
Takashima K, Matsuo S, Fujii T, Hatakenaka N, Kurihara S and Zeilinger A 2009 *J. Phys.: Conf. Ser.* **150** 052260
Fujii T, Matsuo S, Hatakenaka N, Kurihara S and Zeilinger A 2011 *Phys. Rev.* B **84** 174521
[57] Wilson C M, Johansson G, Pourkabirian A, Simoen M, Johansson J R, Duty T, Nori F and Delsing P 2011 *Nature* **479** 376
[58] Casimir H B G 1948 *Proc. R. Neth. Acad. Arts Sci.* **51** 793
[59] Korotaev S M and Kiktenko E O 2010 *AIP Conf. Proc.* **1316** 295
[60] Kiktenko E O and Korotaev S M 2012 *Phys. Lett.* A **376** 820
[61] Korotaev S M and Kiktenko E O 2012 *Phys. Scr.* **85** 055006
[62] Kiktenko E O and Korotaev S M 2013 *Phys. Scr.* **88** 055008
[63] Zyczkowski K, Horodecki P, Horodecki M and Horodecki R 2001 *Phys. Rev.* A **65** 012101
[64] Menzel E P, Deppe F, Mariantoni M, Araque Caballero M A, Baust A, Niemczyk T, Hoffmann E, Marx A, Solano E and Gross R 2010 *Phys. Rev. Lett.* **105** 100401
Mariantoni M, Menzel E P, Deppe F, Araque Caballero M A, Baust A, Niemczyk T, Hoffmann E, Solano E, Marx A and Gross R 2010 *Phys. Rev. Lett.* **105** 133601
[65] Mallet F, Castellanos-Beltran M A, Ku H S, Glancy S, Knill E, Irwin K D, Hilton G C, Vale L R and Lehnert K W 2011 *Phys. Rev. Lett.* **106** 220502
Eichler C, Bozyigit D, Lang C, Steffen L, Fink J and Wallraff A 2011 *Phys. Rev. Lett.* **106** 220503
[66] Wootters W K 1998 *Phys. Rev. Lett.* **80** 2245
[67] Abdalla M S 1994 *Nuovo Cimento* B **109** 443
[68] Müller M E 1959 *Commun. Assoc. Comput. Mach.* **2** 19
Marsaglia G 1972 *Ann. Math. Stat.* **43** 645